Journal of Alloys and Compounds 495 (2010) 348–351

Contents lists available at ScienceDirect

Journal of Alloys and Compounds

journal homepage: www.elsevier.com/locate/jallcom

Effect of temperature on the mechanical behaviour of a Ni-free zirconium-based bulk metallic glass

M. Nascimento [a], J. Ragani [a], S. Gravier [a,*], J.J. Blandin [a], J.L. Soubeyroux [b]

[a] Grenoble-INP, UJF, SIMAP-GPM2, CNRS, 38402 Saint-Martin d'Hères Cedex, France
[b] Institut Néel, CRETA, CNRS Grenoble, France

ARTICLE INFO

Article history:
Received 16 July 2008
Received in revised form 22 October 2009
Accepted 23 October 2009
Available online 31 October 2009

Keywords:
Metallic glasses
Mechanical properties
Crystallization
Biocompatibility

ABSTRACT

It is well known that nickel-free zirconium-based bulk metallic glasses are of interest for their possible good biocompatibility properties. In this framework, a Zr–Nb–Cu–Al–Fe bulk metallic glass was elaborated under the form of 2 mm diameter rods. The amorphous structure was confirmed by XRD and DSC and the associated reduced index were measured. The mechanical properties of the glass were investigated at both room and high temperature. At room temperature, the glass exhibits some macroscopic plasticity. The rheology at high temperature was studied by both strain rate jump tests and tests at constant strain rate. From these tests, it was difficult to identify an experimental window in which the amorphous structure could be maintained and in which viscoplastic forming could be carried out under low flow stresses. In the super-cooled liquid region, this behaviour is discussed in relation with the resistance to crystallization of the investigated glass and the nature of the formed crystallites was studied by XRD. The mechanical properties of this glass are also compared to results previously obtained in the case of other zirconium-based bulk metallic glasses.

1. Introduction

Bulk metallic glasses (BMGs) exhibit interesting mechanical properties since they combine a high fracture stress, a particularly large elastic domain (up to 2%), significant fracture toughness, excellent corrosion resistance and good wear resistance [1–3]. Moreover, their formability between the glass transition temperature, T_g, and the crystallization temperature, T_x, is particularly important and it is thus possible, using appropriate forming processes, to produce complex-shaped components with a very good surface aspect. Thus, the effect of temperature on deformation has been increasingly studied in the recent past, particularly in the case of zirconium-based BMG [4–5]. Consequently BMGs appear has good candidate for biomedical applications. However, two major drawbacks can be pointed out for this kind of application: (i) the Zr-based BMGs usually contain some inclusion of the Ni element, which result in allergy and is potentially carcinogenic to the human body [6–7] (ii) moreover monolithic mechanical behaviour of BMGs is usually considered as brittle since plastic deformation is highly localized in a shear band and often lead to macroscopic brittleness (i.e. the localized plasticity can not be observed macroscopically).

The second drawback is presently being solved through the recent development of many BMGs presenting some macroscopic plasticity; even though the plastic deformation remains localized in multiple shear bands [8–11]. Considering the first drawback, Liu et al. [12] recently developed a new Ni-free Zr-based BMG and demonstrated its good biocompatibility and ability to undergo some plastic deformation. The aim of the present investigation is hence to study the mechanical properties of this glass at room and more especially at high temperature. One of the objectives being to know the possibility to identify an experimental window in which the amorphous structure can be maintained and in which viscoplastic forming can be carried out under relatively low flow stresses.

2. Materials and experimental procedure

In order to elaborate this glass, elements with purity better than 99.9% were used as starting materials. Zr–Nb was first prepared as an intermediate alloy prior to be re-melted with Cu, Fe and Al in order to obtain the master alloy. The $Zr_{60}Nb_5Cu_{20}Fe_5Al_{10}$ bulk metallic glass rods were prepared by casting the melt in a copper mould with a 2 mm diameter cooled with water circulation. The structure of the alloy was studied by X-Ray diffractometer (XRD) with CuKα radiation. The thermal glass stability was determined by differential scanning calorimetry with a heating rate of 20 K/min. (Perkin Elmer Diamond). After each run, a second run was performed in order to estimate the baseline. From DSC analyses, the characteristic temperatures T_g (glass transition temperature) and T_x (onset of crystallization) were measured. TEM samples were prepared using wire saw in order to get few tens of microns foils that were finally thinned down to observation thickness by ion milling.

* Corresponding author. Tel.: +33 476826379.
E-mail address: sebastien.gravier@simap.grenoble-inp.fr (S. Gravier).

0925-8388/$ – see front matter © 2009 Elsevier B.V. All rights reserved.
doi:10.1016/j.jallcom.2009.10.186

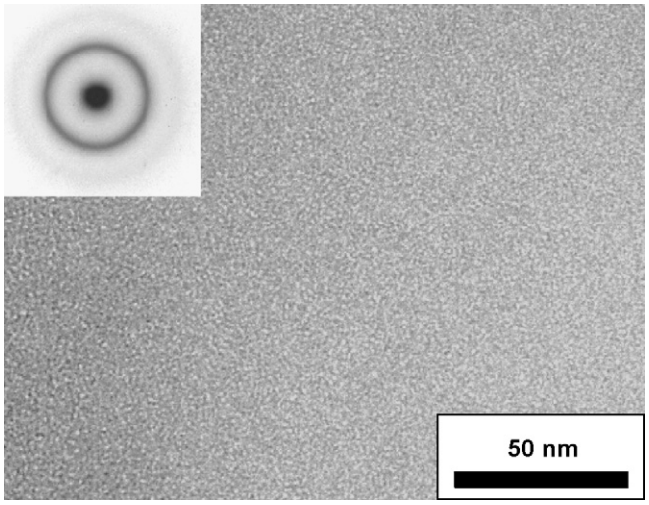

Fig. 1. TEM image and associated SAED pattern of the as cast $Zr_{60}Nb_5Cu_{20}Fe_5Al_{10}$ alloy.

The mechanical properties were investigated at room temperature by compressive tests with a strain rate equal to $1 \times 10^{-4}\ s^{-1}$. High temperature deformation was studied by compression tests in air. The samples were heated to the testing temperatures at a heating rate of 20 K/min and held at the testing temperature for about 360 s to homogenize temperature before starting compression. During testing, the temperature was stabilized with an accuracy of less than 1 K. A thin superficial oxidized layer appears during testing but to thin to affect the macroscopic behaviour. The temperature range of interest was between 663 K and 708 K. Compression rods were in both cases cylinder of 2 mm diameter and 3 mm height.

3. Results and discussion

The amorphous structure of the alloy was first confirmed by XRD analysis performed on cross sections of the elaborated rods. This structure was further investigated by TEM, as illustrated by Fig. 1 which shows a contrast-less feature in bright field image and diffused diffraction rings, in the selected area diffraction pattern. Fig. 2 displays a DSC curve of the as cast alloy at a heating rate of 0.33 K/s. One can see the characteristic step changes arising from the glass transition followed by a super-cooled liquid region and then three exothermic peaks associated to three crystallization events. The characteristic temperatures and associated crystallization energies extracted from the DSC analysis are summarized in Table 1. In a first analysis it seems that the ΔT value obtained using the difference between glass transition temperature T_g^{onset} and the onset of crystallization temperature T_x is quite high suggesting a pretty good resistance to crystallization of the investigated glass. It can be noted that the DSC curve is in good accordance with the one obtained on the same BMG by Liu et al. [12] except for the glass transition that is more pronounced in the present study.

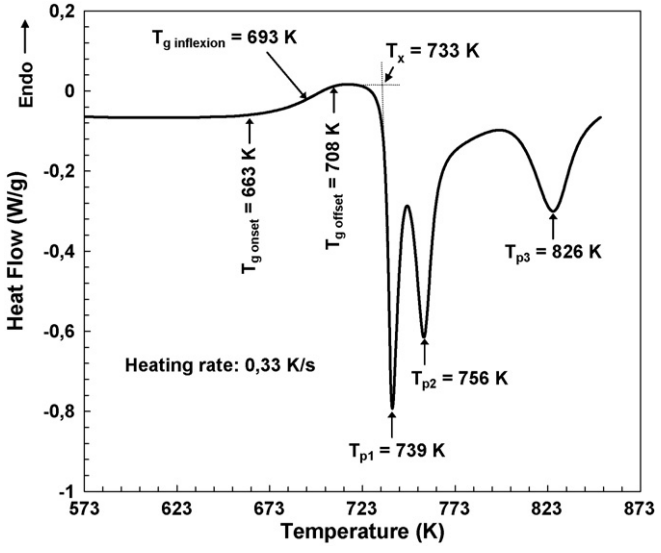

Fig. 2. Differential scanning calorimetric (DSC) curve of $Zr_{60}Nb_5Cu_{20}Fe_5Al_{10}$ metallic glass at a heating rate of 0.33 K/s. The T_g^{onset}, $T_g^{inflexion\ point}$, T_g^{offset} representing respectively the onset, the inflexion point and the offset temperatures of the glass transition, are pointed out. The T_x T_{p1}, T_{p2} and T_{p3} corresponding respectively to the onset of crystallization, the crystallization peaks temperatures of the first, second and third peak, are also quoted.

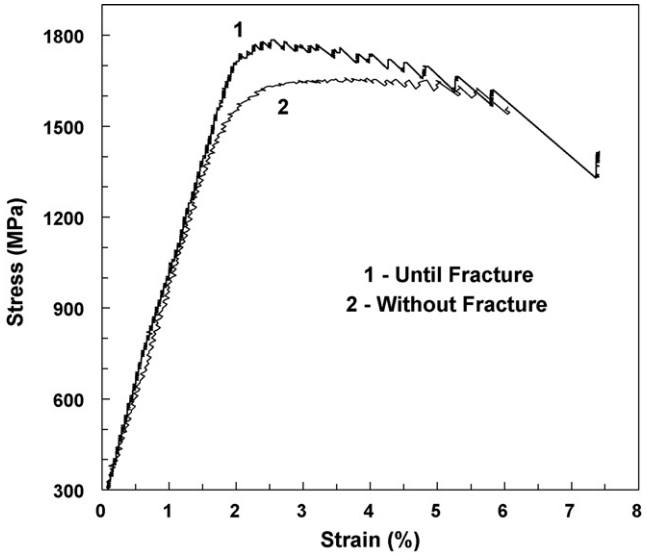

Fig. 3. Stress–strain curve of amorphous $Zr_{60}Nb_5Cu_{20}Fe_5Al_{10}$ at room temperature. Sample 1 is tested until failure and sample 2 was stopped just before its failure.

The room temperature mechanical properties of the as cast sample were studied by compression test and Fig. 3 shows the resulting stress–strain (σ–ε) curves. It is to be noted that the sample 1 was tested until fracture whereas the test concerning the sample 2 was stopped just before its fracture. Maximum strengths between roughly 1600 MPa and 1800 MPa were measured with elastic strains of about 1.6%. All the tested samples displayed some macroscopic plasticity, with a plastic strain of about 5%. These values are in relatively good agreement with the data published very recently by Liu et al. [12]: in their work, a maximum strength of about 1800 MPa was also reported associated to a maximum plastic strain of about 9%.

As expected, some serrations can be detected on the (stress, strain) curves and those serrations are becoming greater when the sample approaches from fracture. Observation of the surface of the tested rod after the test display, as expected, a large number of shear bands confirming the localized plasticity mechanism. Fig. 4(a) shows a SEM observation of the fracture surface of sample 1. Some veins can be detected but not as clearly as it can be frequently observed in various Zr-based BMGs. As expected, the macroscopic plasticity is associated to the development of numerous shear bands in the sample, as illustrated by Fig. 4(b) showing a lateral observation of the sample 2. In particular, a series of five parallel shear bands can be clearly observed, the distances between the bands being quite similar, close to 100 μm. These bands are also oriented at about 45° with respect to the compression axis.

Table 1
Characteristic temperatures and values from DSC measurement on $Zr_{60}Nb_5Cu_{20}Fe_5Al_{10}$ as cast sample at a scanning rate of 20 K/min.

T_g^{onset} (K)	$T_g^{inflexion\ point}$ (K)	T_g^{offset} (K)	T_x (K)	T_{p1} (K)	T_{p2} (K)	T_{p3} (K)	ΔT (K) $= T_x - T_g^{onset}$	Crystallization's Energy (ΔH) for peaks 1 and 2 (J/g)	Crystallization's Energy (ΔH) for peak 3 (J/g)
663	693	708	733	739	756	826	70	43.7	14.3

To our knowledge, no information has been published concerning the high temperature deformation of the $Zr_{60}Nb_5Cu_{20}Fe_5Al_{10}$ metallic glass. In order to get such information, strain rate jump tests were performed at temperatures ranging from 673 to 693 K (keeping in mind that $T_g^{onset} = 663$ K) and with strain rates ranging from 2.5×10^{-4} s^{-1} to 2.5×10^{-3} s^{-1}. Fig. 5 shows the resulting variations of stress with strain rates when the tests were carried out at 673 K and 683 K. One must report that the thermal stability was to poor at 693 K to be able to carry out the whole test. At low strain rates, relatively constant flow stresses were quickly reached whereas at higher strain rates, some stress overshoots could be detected (e.g. at 10^{-3} s^{-1} and 673 K).

From these tests, viscosities were calculated and Fig. 6 displays the variations with the temperature and the applied strain rate of these viscosities. The curves show the typical shape of viscosity in amorphous materials with a viscosity approaching a Newtonian regime (i.e. viscosity independent of the strain rate) for the lower attainable strain rates and a decrease of the viscosity when strain rate increases. It can however be noted that, due to the relatively short experimental window before crystallization, strain rate low enough to clearly identify the Newtonian regime could not be achieved.

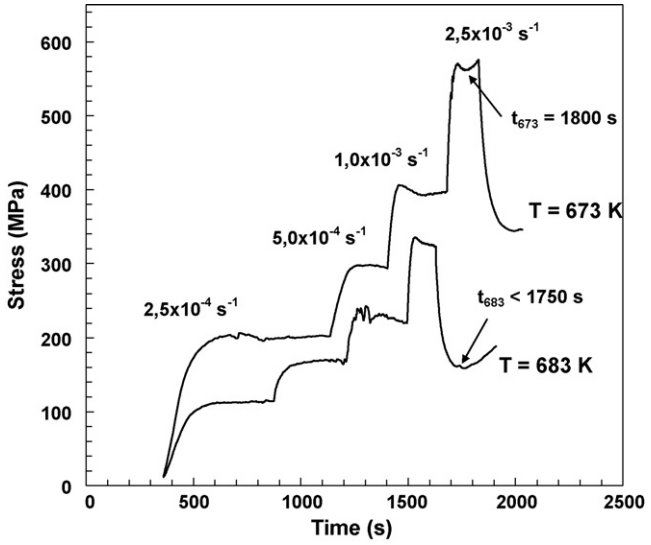

Fig. 5. Stress as a function of total annealing time at two different temperatures for the various indicated strain rates at 673 K and 683 K. Arrows indicating the time where flow stress increases are also represented.

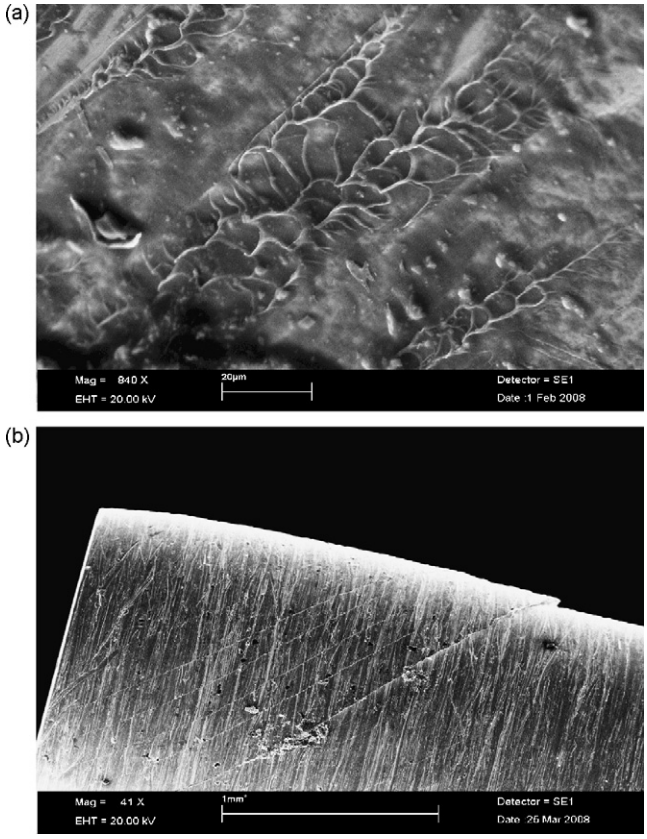

Fig. 4. SEM observations of the deformed samples.
(a) fracture zone.
(b) lateral view of the sample 2 deformed without fracture.

During the strain rate jump tests, apparent strain hardening can be detected at the end of the tests. Such hardening is attributed to partial crystallization which is expected to occur in the alloy. To confirm this hypothesis, a test at a constant strain rate of 2.5×10^{-3} s^{-1} was carried out at 693 K. A strong increase of the flow stress can be observed after a given time as illustrated by Fig. 7: the flow stress remains roughly constant close to 150 MPa at the beginning of the test and then a reinforcement factor of about 4 is obtained after less than 8 min. The hardening occurs after a time

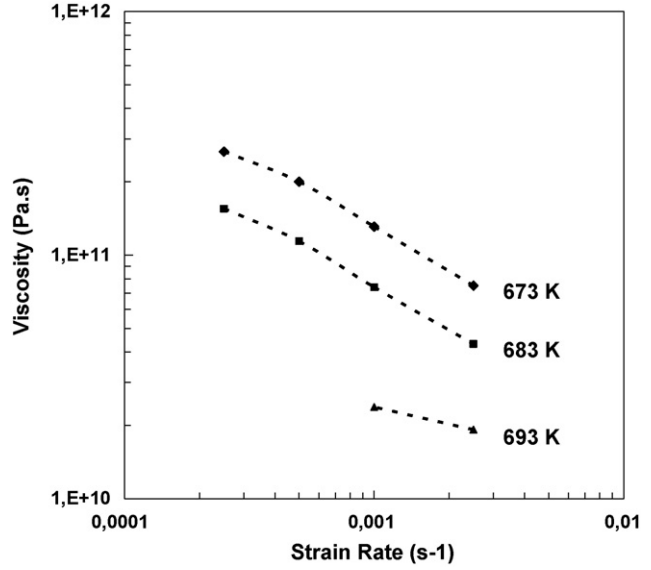

Fig. 6. Viscosity versus Strain rate curves for $Zr_{60}Nb_5Cu_{20}Fe_5Al_{10}$ deduced from the strain rate jump tests at three different temperatures.

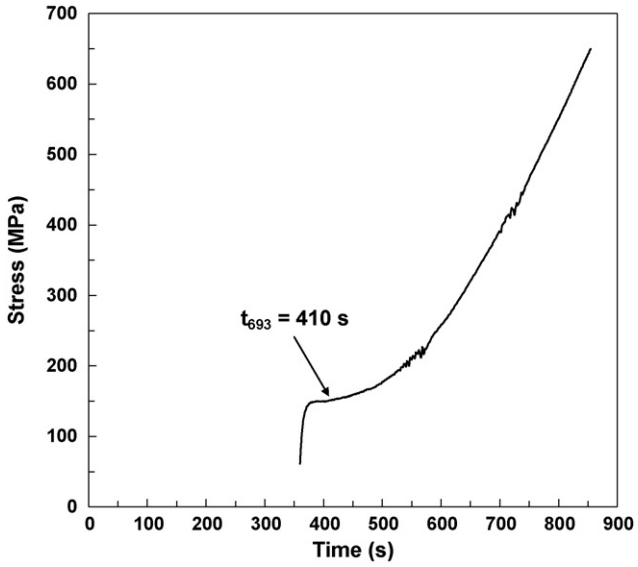

Fig. 7. Stress as a function of total annealing time at 693 K at a constant strain rate of 2.5×10^{-3} s^{-1}.

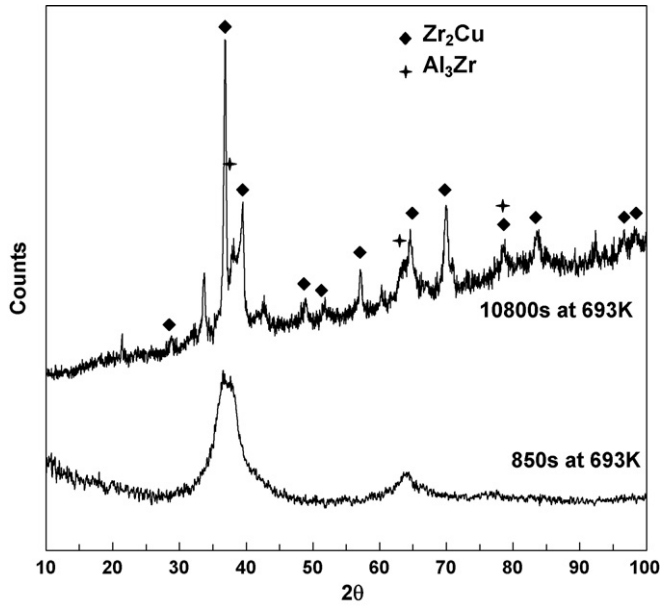

Fig. 8. X-Ray diffraction curves for the sample annealed 850 s at 693 K while deforming at a strain rate of 2.5×10^{-3} s^{-1} and for a sample annealed 10,800 s (3 h) at a temperature of 693 K.

$t \approx 410$ s. At lower temperatures, similar critical times for crystallization can be detected, as illustrated by Fig. 5: at 673 K, $t \approx 1800$ s whereas $t < 1750$ s at 683 K. Fig. 8 displays the XRD obtained on the sample after the test at 693 K and confirm the partial crystallization of the sample since some diffuse peaks are appearing. However, it was not possible to index clearly the crystallized phases. In order to investigate in more details the crystallization process, a longer heat treatment of 3 h at 693 K was performed. A DSC scan was then performed on the treated sample showing that the annealing corresponded to the vanishing of the two first crystallization peaks while the third crystallization peak observed on the amorphous sample was not modified. Indeed, a remaining crystallization energy for the two first crystallization peaks of 2.4 J/g is measured. The resulting XRD curve corresponding to this heat treatment of 3 h at 693 K is also displayed in Fig. 8 and some phases could be identified as Zr_2Cu or Al_3Zr.

4. Conclusions

The mechanical properties of a Zr-based BMG candidate for biomedical applications have been tested. Some macroscopic plasticity, localized in shear bands, is observed at room temperature. Around the glass transition, as expected, large deformation ability is measured corresponding to a good forming ability. The major drawback to the use of this BMG is its poor resistance to crystallization leading to an experimental window for injection process relatively limited. Resistance to crystallization is an important point for the forming process (and consequently for the use of BMG) which is often neglected.

Acknowledgment

The authors would like to acknowledge Patricia Donnadieu for her help in the analysis of the TEM samples.

References

[1] C.J. Gilbert, R.O. Ritchie, W.L. Johnson, Appl. Phys. Lett. 71 (1997) 476.
[2] S.J. Pang, T. Zhang, H. Kimura, K. Asami, A. Inoue, Mater. Trans. JIM 41 (2000) 1490.
[3] J.G. Wang, B.W. Choi, T.G. Nieh, C.T. Liu, J. Mater. Res. 15 (2000) 913.
[4] B. Guo, X.L. Guo, M.Z. Ma, D.B. Shan, W.W. Zhang, J. Non-Cryst. Solids 354 (2008) 3348–3353.
[5] L. Liu, Q. Chen, K.C. Chan, J.F. Wang, G.K.H. Pang, Mater. Sci. Eng. A 449–451 (2007) 949–953.
[6] P.J. Uggowitzer, R. Magdowski, M.O. Speidel, ISIJ Int. 36 (1996) 901–908.
[7] J.C. Wataha, P.E. Lockwood, A. Schedle, J. Biomed. Res. 52 (2000) 360–364.
[8] J. Schroers, W.L. Johnson, Phys. Rev. Lett. 93 (2004) 255506.
[9] Y.H. Liu, G. Wang, R.J. Wang, D.Q. Zhao, M.X. Pan, W.H. Wang, Science 315 (2007) 1385.
[10] Y.K. Xu, H. Ma, J. Xu, E. Ma, Acta Mater. 53 (2005) 1857–1866.
[11] A.V. Sergueeva, N.A. Mara, J.D. Kuntz, D.J. Branagan, A.K. Mukherjee, Mater. Sci. Eng. A 383 (2004) 219–223.
[12] L. Liu, C.L. Qiu, Q. Chen, K.C. Chan, S.M. Zhang, J. Biomed. Mater. Res., Part A 86A (1) (2008) 160.